IET Electric Power Applications

Special Issue: Advances in Multi-MW Wind Energy Conversion Systems

IET Journals
The Institution of Engineering and Technology

Series-connected multi-half-bridge modules converter for integrating multi-megawatt wind multi-phase permanent magnet synchronous generator with dc grid

ISSN 1751-8660
Received on 27th September 2016
Revised on 15th December 2016
Accepted on 31st January 2017
doi: 10.1049/iet-epa.2016.0653
www.ietdl.org

Ahmed A. Elserougi[1,2] ✉, Mohamed I. Daoud[3], Ayman S. Abdel-Khalik[2], Ahmed Mohamed Massoud[3], Shehab Ahmed[1]

[1]*Electrical and Computer Engineering Department, Texas A&M University, Doha, Qatar*
[2]*Department of Electrical Engineering, Alexandria University, Alexandria, Egypt*
[3]*Electrical Engineering Department, Qatar University, Doha, Qatar*
✉ *E-mail: ahmed.elserogi@qatar.tamu.edu*

Abstract: In this study, a new transformerless wind energy conversion system to integrate high-power multi-phase permanent magnet wind generators to medium-voltage local grids is presented. The proposed converter topology consists of multi-half-bridge modules with a high ac–direct current (dc) boosting capability. Each phase of an open winding multi-phase generator is connected to the ac side of a half-bridge module, whereas the dc sides of the half-bridge modules are connected in series forming the high-voltage dc-link output. The proposed architecture facilitates the employment of semiconductor switches with a relatively low-voltage rating, which equals the dc-link voltage divided by the number of generator phases. A detailed analysis of the proposed architecture along with the required closed-loop control is presented. The proposed architecture is simulated under different operating conditions using a typical 2 MW system, while the experimental validation is carried out using a low-scale prototype converter.

1 Introduction

The ever-growing energy demand along with the depletion of the conventional energy resources have led to a high penetration of renewable energy sources. Wind energy (WE) is considered as a main promising renewable energy source with an approximate capacity of 300 GW worldwide [1]. Owing to the massive offshore wind resources, offshore wind farms' energy conversion development has seen intense research work recently. The main design elements of a WE conversion system (WECS) are the electric generator, the power converter, and the control strategy. Multi-megawatt (MW) wind turbines have been targeted in offshore wind farms with a low-voltage high-current power generation trait (for example, 690 V rated voltage and 1–10 MW rated power [1]). The higher the turbine rating, the lower the energy cost of the offshore wind power will be [2]. Therefore, several constructions and techniques of the electric generator and power converter have been proposed in the literature considering high-power ratings.

To meet the requirement of the low-voltage bulk-power generation peculiarity of the WECS, a single power converter cannot be used. Therefore, parallel-converters configuration has been proposed in the literature [3–11]. The main drawbacks of the parallel operation are the low-voltage operation, which requires a step-up stage through a transformer or a direct current (dc)–dc boost converter in order to be able to connect to a medium-voltage dc grid, and the presence of circulating currents, which do not only increase the power losses but also challenge the power sharing control of different converters [7, 11].

The presence of a step-up transformer in offshore wind turbines is considered a technical drawback as it enlarges the size of the nacelle, in addition to its maintenance requirements [1, 2]. On the other hand, high-power step-up dc–dc conversion is required in case of low-voltage operation with no transformer installed in order to meet the required transmission voltage level [12, 13]. The presence of a dc–dc converter increases the number of conversion stages, which adds up to the system power losses and cost, and affects the system reliability. Consequently, transformerless-based systems have been targeted in order to improve the wind turbine construction, maintenance requirements, and power losses. Special generator segments connected to a cascaded H-bridge converter was proposed in [14, 15] to provide a transformerless operation. Another topology using series-connected three-level neutral-point-clamped (NPC) converters was introduced in [16]. The use of modular multilevel converters (MMCs) for transformerless wind–grid integration has shown promise in [17]. While in [18], a boost converter is used to elevate the output voltage of the diode rectifier connected to the wind turbine to the grid voltage level.

Recently, multiple three-phase winding generators have been introduced for WECSs for ease of power sharing purposes for both series and parallel operations [2, 19–23]. In series-connection, the output of each three-phase set is connected to a voltage source converter (VSC), and then their dc outputs are connected in series to form a high-voltage dc (HVDC) link without the need for a transformer or a dc–dc boosting stage.

Whilst doubly fed induction generators have been widely used in WE applications, the recent wind generation topologies are trended to permanent magnet synchronous generators (PMSGs) due to their higher efficiency and larger torque density. In WE conversion, multi-phase machines outweigh their conventional three-phase counterparts, thanks to their high fault tolerance capability, lower torque ripple, and lower power rating requirement per-phase. In [19], a dual-three-phase induction machine (IM) with series-connected converters for each three-phase set is applied, which provides double the dc-link voltage level compared with three-phase converters connected to conventional three-phase machines. In [2], a nine three-phase segment generator is connected to nine three-phase VSC modules with the output connected in series to form a 100 kV dc-link voltage output.

In this paper, a new transformerless WECS is proposed for integrating multi-MW multi-phase PMSG with medium-voltage

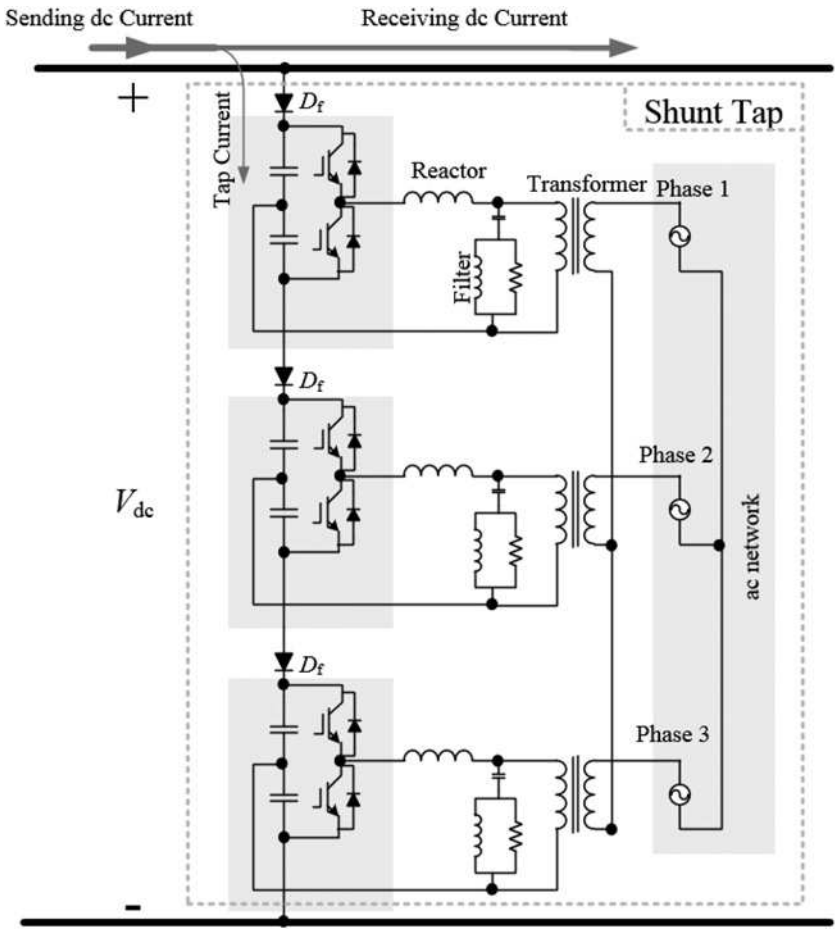

Fig. 1 *HVDC shunt tap proposed in [24]*

local wind farm grids, where the obtained ac–dc voltage boosting is enough to produce the required dc-link voltage (3–4 kV), typical voltage level for local electrical connection within a wind farm [18]. The presented approach has been inspired from the HVDC shunt tap presented in [24] by ABB but with a different perspective.

This HVDC tap architecture is shown in Fig. 1, which consists of six series-connected dc capacitors connected across the dc bus. Ideally, the voltage of each capacitor equals to the total dc voltage divided by the number of series-connected capacitors (i.e. $V_c = V_{dc}/6$).

Each two successive dc-capacitors are used to feed a two-level half-bridge converter. Each half-bridge converter feeds one-phase of the three-phase load. The voltage profile of each phase is a bipolar voltage ($\pm V_{dc}/6$), with a fundamental component peak of $MV_{dc}/6$, where M is the peak of the sinusoidal modulating signal and $0 < M \leq 1$. This arrangement has a bucking capability from the dc side to the ac side (i.e. inversion mode). Extra protecting diodes (D_f) have been used in this topology to block the current flow from the ac network (tap) into the dc-link during dc line faults. However, in order to permit a bidirectional power flow, these blocking diodes should be eliminated. In this paper, the same concept is applied for integrating multi-phase PMSG to a dc bus. A case study for integrating an asymmetrical six-phase PMSG is presented. The same previous topology when operating in the rectification mode provides a high ac–dc boosting capability which provides a transformerless operation. For a six-phase case, the dc-link voltage level will be 12 times the converter peak phase voltage under unity peak modulating signals ($M = 1$).

Generally, for an m-phase generator, the proposed converter will comprise m half-bridge converters and $2m$ dc capacitors. Ideally, the voltage of each dc capacitor equals $V_{dc}/2m$, while the peak of the fundamental output voltage of each half-bridge converter equals $V_{dc}/2m$ under unity peak modulating signals. This ends up with a boosting ratio of $2m$.

The main expected advantages of the proposed architecture are:

(i) The proposed topology can offer a transformerless operation with an ac–dc boosting gain of $2m$ when integrating an m-phase generator.
(ii) The operation with a relatively low-voltage rating semiconductor switches. Hence, the complexity and challenges of series-connection of semiconductor devices are avoided.
(iii) Each phase can be controlled independently, i.e. modular controller can be adopted, which reduces the complexity of the controller tuning.

The main challenges of the proposed approach are also discussed with suggested solutions throughout this paper. Table 1 summarises the advantages and disadvantages of the proposed approach compared with other available topologies.

Simulation case study for a typical 2 MW asymmetrical six-phase PMSG with the proposed architecture is presented to check the viability of the proposed approach. Finally, the experimental validation for the proposed converter is carried out using an available dual-three-phase IM-based flywheel energy storage system. The IM can be operated in generation mode during the discharging periods of the flywheel, emulating the wind turbine. The simulation and experimental results elucidate the theoretical claims.

2 Proposed architecture

2.1 Converter topology

The proposed configuration for integrating a six-phase PMSG with dc grid is shown in Fig. 2. The proposed converter consists of six

IET Electr. Power Appl., 2017, Vol. 11, Iss. 6, pp. 981–990

Table 1 Advantages and disadvantages of the proposed approach compared with other topologies

Converter topology	Advantages	Disadvantages
parallel-converters [9]	• employing multi-converter with reasonable power rating in low-voltage bulk-power wind generation applications	• it requires a step-up stage through transformer or dc–dc boost converter, which affects the system losses and volume • owing to parallel-connection, the circulating currents may increase the system losses and affect the power sharing control of the different involved converters
transformerless cascaded H-bridge converter [14]	• operating with identical coils and converter modules (low cost) • high reliability	• employment of active rectifiers for coils to have the ability of controlling each of the dc-link average voltages • system complexity (plenty of switches are involved) • large number of involved switches and capacitors
transformerless MMC [17]	• modularity • scalability • efficient operation	• capacitors voltages and circulating currents should be controlled in addition to the active and reactive powers (i.e. complex control)
three-level boost converter and NPC-based system [18]	• simple, low cost, and reliable • the two dc output voltages of the three-level boost converter can be used effectively to feed three-level NPC converter • operating with significant improvement in the grid power quality	• it is a two-stage configuration that may affect the overall system efficiency
transformerless series-connected three-phase VSCs with multi-phase generator [2]	• having ac–dc boosting capability	• series-connection problems (fault and insulation level) • multi-module three-phase VSCs need a large number of controlled switches
the proposed topology: transformerless series-connected single-phase half-bridge VSCs with multi-phase generator	• having high ac–dc boosting capability • moderate number of switches with reasonable voltage rating	• series-connection problems (fault and insulation level) • relatively large dc-link capacitances are required

half-bridge converters, their dc sides are connected in series, while the ac side of each half-bridge converter is connected to one-phase of an open winding asymmetrical six-phase PMSG. Each half-bridge converter controls the phase current of the corresponding generator phase. The voltages of the dc capacitors (12 capacitors in case of a six-phase PMSG) are also controlled to ensure an equal voltage sharing. The voltage share of each capacitor equals ($V_{dc}/12$), which results in a phase voltage magnitude of $MV_{dc}/12$.

It is clear that the proposed configuration has a good boosting capability from the ac to dc side; hence, a relatively low-voltage PMSG can directly be coupled to a medium-voltage dc link (V_{dc}) without an extra voltage boosting stage. The main advantages and challenges of the proposed architecture are mentioned clearly in the following section.

2.2 Advantages and challenges of the proposed converter

The proposed converter provides the following advantages:

(i) Operation with a relatively high ac–dc boosting capability (1:2m), where m is the number of generator phases, when compared with the available topologies in the literature.

(ii) A relatively low-voltage rating semiconductor switches can be employed for a given high dc-link voltage level.
(iii) Modular controllers can be employed, as each phase can be independently controlled.

Also, some challenges are imposed when such an architecture is employed, which are:

(i) The insulation level of different generator phases will be different due to the series-connection of the dc-link capacitors. The lower winding (the nearest winding to the negative pole of the dc-link voltage) will have a lower insulation level: namely, V_{dc}/m, whereas the upper winding (the nearest winding to the positive pole of the dc-link voltage) will have the highest insulation level which is V_{dc}. The insulation level of different winding sets increases gradually with a step of V_{dc}/m from the lower to the upper windings. This will impose technical challenges if conventional double-layer distributed winding is adopted, which is the practical case for conventional high-power generators. Recently, the non-overlapped fractional slot concentrated winding (FSCW) layouts [25] offer many outstanding merits in the design of direct-drive PM wind generators with high diameter and, therefore weight, including improved torque and power densities, lower copper volume due to the significant reduction in the end

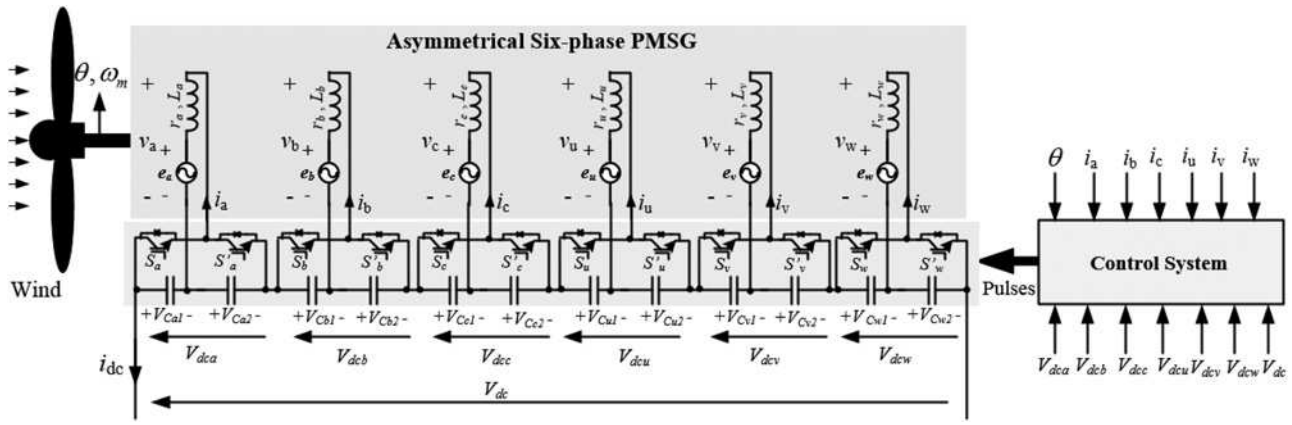

Fig. 2 *Proposed WECS*

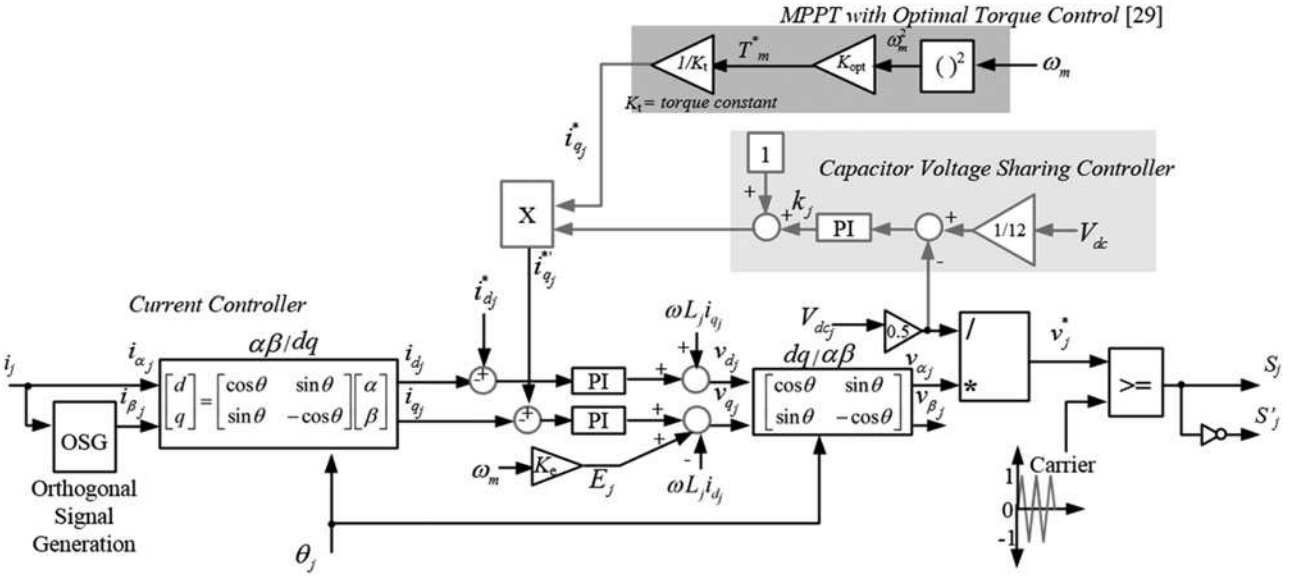

Fig. 3 *Per-phase controller of the proposed architecture*

turn winding volume, higher filling factor, and high torque and voltage qualities, critical requirements of high-power direct-driven wind generators [26]. Besides, FSCWs allow for a modular machine from the construction point of view, which facilities the generator manufacturing and provides a more cost-effective design for such heavy generators [27]. Fortunately, the modular construction with an adopted single-layer winding facilitates the winding insulation process and can be a practical example where the proposed converter can be applied. For certain slot/pole combinations, a complete physical separation between phases can be obtained, which highly simplifies the electrical insulation of different phases [28].

(ii) Each phase of the PMSG is connected between the mid-point of the converter leg and the mid-point of the common point between each pair of capacitors. Hence, the phase current will circulate through these capacitors, which corresponds to a notable voltage ripple component superimposed on the capacitors' voltages. This voltage ripple component depends on the operating frequency, phase current magnitude, and the capacitance value. The average dc voltage level across each capacitor equals $V_{dc}/(2m)$ while the frequency of this superimposed voltage ripple component equals the fundamental frequency. Increasing the capacitance can be a simple and direct solution to reduce this ripple voltage; however, this may end up with high capacitance values for low-voltage high-power systems. By thoroughly investigating this problem, it has been found that there is a relation between the capacitance value and the fundamental phase voltage magnitude. As the capacitance value decreases, the fundamental phase voltage increases for the same peak of the modulating signal. This is mainly due to the fact that the induced voltage ripple component has the same fundamental frequency. On the other hand, a low value of the dc-link capacitors corresponds to a higher ripple current magnitude at the dc side. Hence, a compromise should be made in the converter design between the acceptable dc-link current ripple and the minimum capacitance that maybe employed. To highlight the effect of the capacitance value on the output voltage magnitude, a simulation case study will be presented in Section 4.

(iii) One of the main problems of converter topologies based on series-connection is the relatively low fault tolerant capability. A failure in one if the series modules yield a complete system shutdown. As a possible remedy to this problem, the system can be equipped with redundant modules that are bypassed during normal operating condition. In case of a module failure, one of these redundant modules can be used as a replacement [2].

3 Control system

The per-phase controller of the proposed configuration is shown in Fig. 3, where j denotes the phase letter ($j = a$, b, c, u, v, and w in case of the six-phase system). The control system is divided into three controllers: namely, maximum power point tracking (MPPT) control, current controller, and capacitor voltage sharing controller. The details of each controller stage are illustrated in the following sections.

3.1 MPPT control

MPPT controller in WECS is an essential block to extract the maximum achievable WE at all conditions. Among different MPPT techniques of WECSs, optimal torque control [29] is

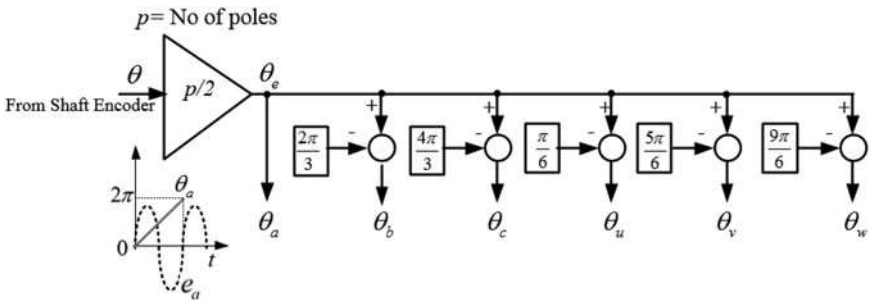

Fig. 4 *Extracting the orientation of generator phases*

IET Electr. Power Appl., 2017, Vol. 11, Iss. 6, pp. 981–990

Table 2 Simulation data

Parameters	Values
PMSG specifications	2 MVA, asymmetrical six-phase PMSG, and nominal frequency = 50 Hz
per-phase inductance of the winding	200 μH
per-phase resistance of the winding	0.3 mΩ
per-phase voltage peak at the rated speed	200 V
i_{qj}^* and i_{dj}^*	−3000 A (rated) and 0 A, respectively
dc-link capacitances	case 1: 200 mF (high capacitance), case 2: 50 mF (lower capacitance)
dc voltage at the receiving side	4 kV (transmission impedance: 0.1 Ω in series with 0.1 mH)
carrier frequency for each half-bridge converter	5 kHz
PI-controllers (current controllers)	$k_p = 0.5$ and $k_i = 20$
PI-controllers (dc voltage controllers)	$k_{pc} = 0.001$ and $k_{ic} = 0.1$

applied in this work. Detailed illustration for this MPPT technique can be found in [29]. Generally, the MPP trajectory is given by

$$P_m = k_{opt}\omega_m^3 \tag{1}$$

where P_m and ω_m are the mechanical power and speed of the wind turbine, respectively.

The optimal coefficient k_{opt} depends on the wind turbine parameters. Hence, the optimal torque reference can be expressed by

$$T_m = k_{opt}\omega_m^2 \tag{2}$$

The optimal torque reference is then used to obtain the required quadrature current component. In low-speed PM generators, it is a common practise to set the dc component to zero.

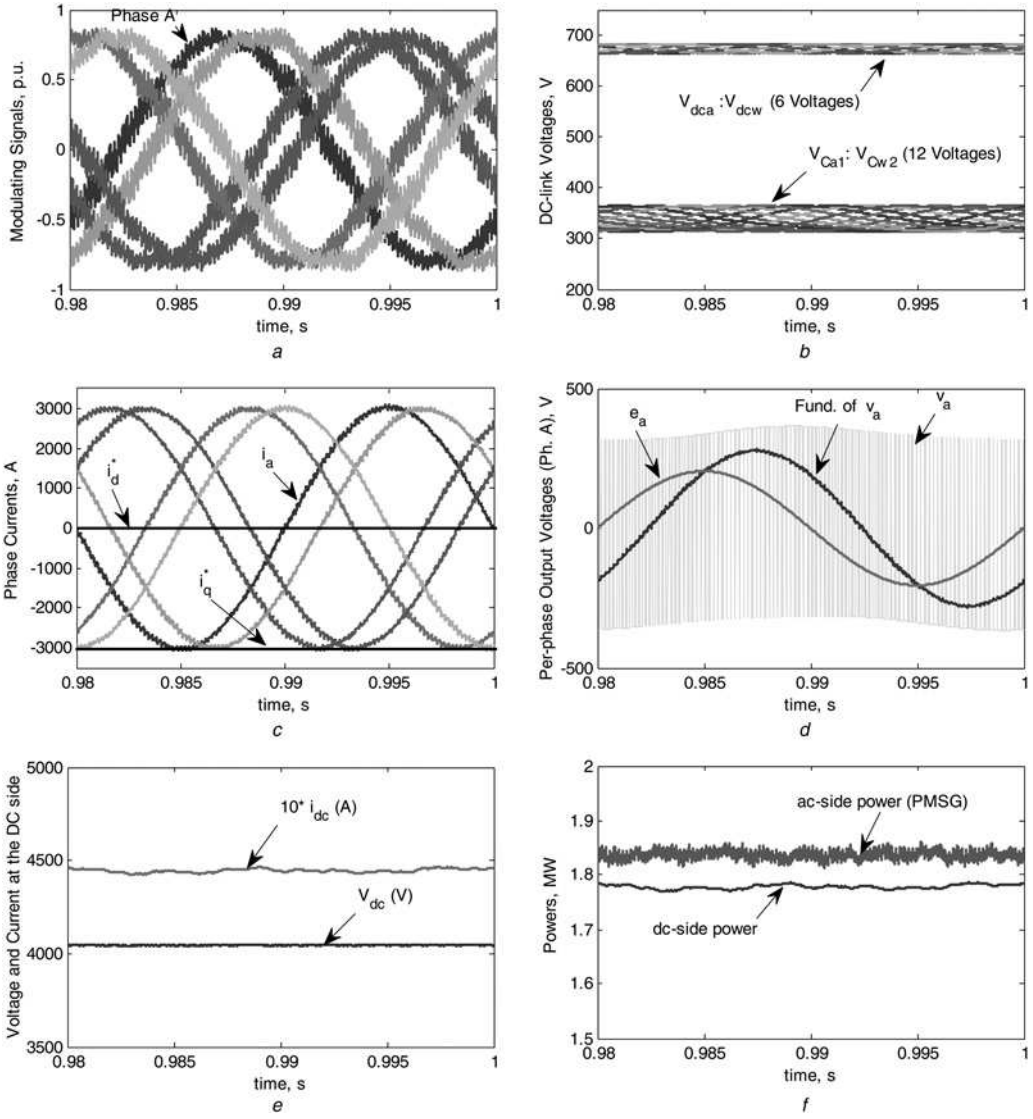

Fig. 5 *Simulation results for a high dc-link capacitance (200 mF) at rated frequency*

a Modulating signals of the involved half-bridge converters
b dc-Link voltages
c Phase currents
d Per-phase output voltages (phase A)
e dc Voltage and scaled-up current at the dc terminals of the proposed architecture
f Input (ac side) and output (dc side) powers

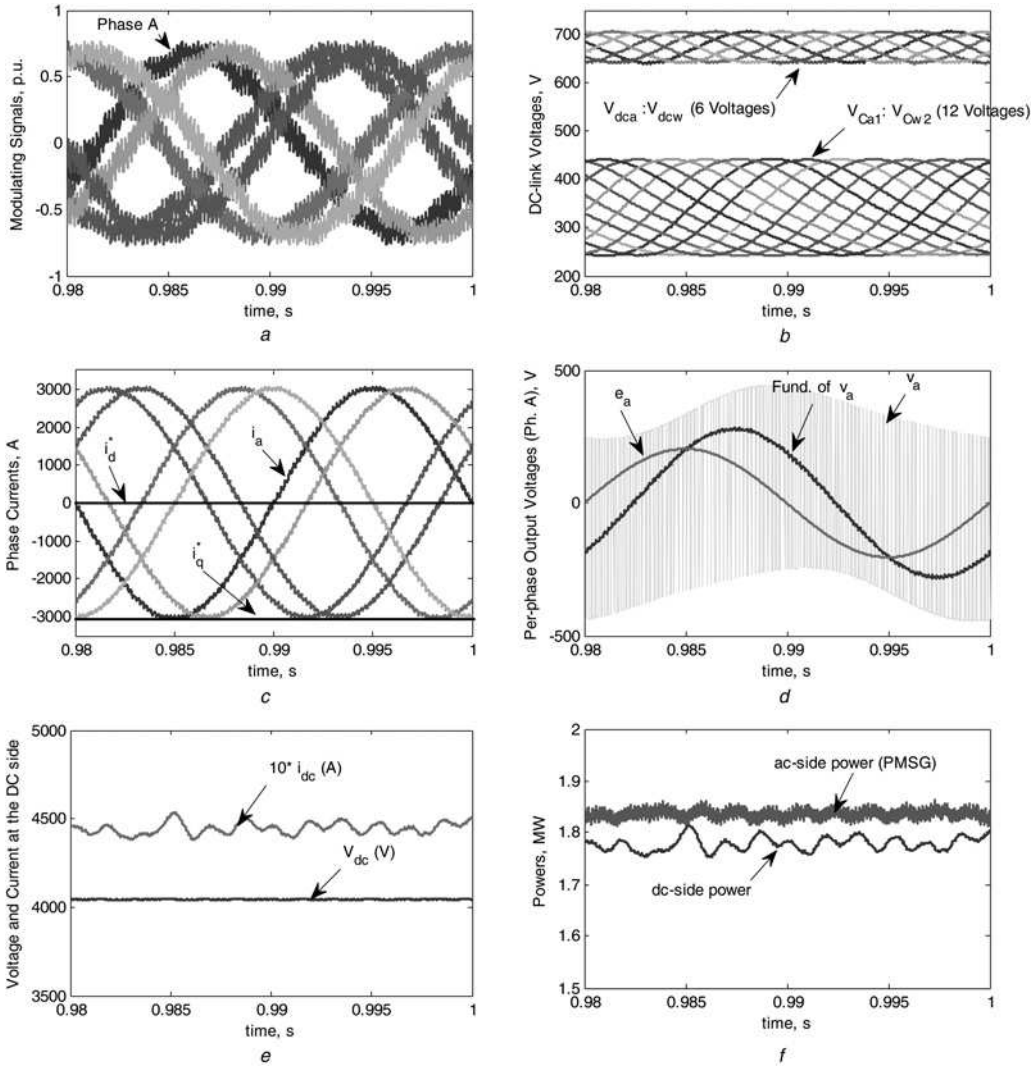

Fig. 6 *Simulation results for a low dc-link capacitance (50 mF) at rated frequency*

a Modulating signals of the involved half-bridge converters
b dc-Link voltages
c Phase currents
d Per-phase output voltages (phase A)
e dc Voltage and scaled-up current at the dc terminals of the proposed architecture
f Input (ac side) and output (dc side) powers

3.2 Current controller

Since all phases are independently controlled and to ensure a proper current tracking, two proportional–integral (PI) controllers are used to control the current of each phase as shown in Fig. 3. First, the current of any phase (i_j) is measured and considered as the α-component of this phase current, whereas the β-component of current is extracted via employing an orthogonal signal generator [30], typically employed to facilitate a dq power control for single-phase systems. These $\alpha\beta$ current components are then transformed to their synchronous dq current components. The synchronisation angle of each phase (θ_j) is obtained as shown in Fig. 4. On the basis of Fig. 3, two PI controllers are used to determine the dq voltage components. Then, dq voltage components can be transformed into $\alpha\beta$ voltage components. The extracted α-component of the voltage divided by $0.5V_{dcj}$ represents the reference modulating signal for the half-bridge converter for phase (j) [30].

Owing to the series-connection of the dc capacitors, the instantaneous values of the dc sides of different half-bridge converters are not equal. Hence, each dc capacitor voltage should be measured to calculate the suitable modulating signal for each phase. Finally, conventional sinusoidal pulse-width modulation (PWM) can be simply employed to control the voltage of each phase based on the extracted per-phase reference modulating voltage signal (v_j^*).

3.3 Capacitor voltage sharing controller

The total dc voltage level (V_{dc}) is generally controlled using the grid-side converter (GSC), which is not presented in the current paper. Consequently, the dc-link mid-points will be floating, and the GSC controller cannot be used to ensure an equal voltage sharing. This necessitates an additional controller to ensure equal voltage levels across the different cascaded dc-link capacitors. The concept of dc capacitor voltage sharing controller presented in [31] can be simply employed herein. In this controller, half the value of the per-phase dc-side voltage ($V_{dcj}/2$) is compared with the total dc voltage divided by the total number of dc capacitors (12 in case of the six-phase PMSG). A PI-controller is then used to generate the required correction factor (k_j) which is used to continuously change the quadrature component of the corresponding reference current to ensure equal voltage distribution in case of any possible mismatch, as shown in Fig. 3.

IET Electr. Power Appl., 2017, Vol. 11, Iss. 6, pp. 981–990

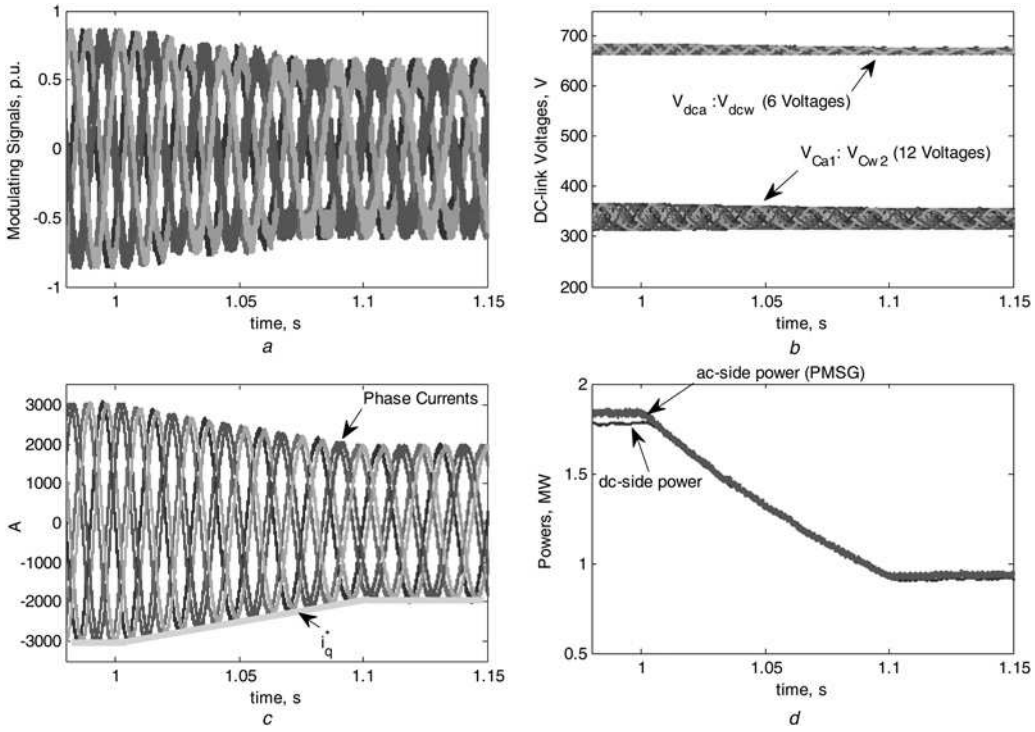

Fig. 7 *Dynamic performance of the system after reduction of mechanical speed*

a Modulating signals of the involved half-bridge converters
b dc-Link voltages
c Phase currents
d ac Side and dc side powers

4 Simulation

In this section, the system performance of a typical 2 MW generator is simulated using MATLAB/Simulink. A simulation model has been built for the proposed asymmetrical six-phase WECS architecture as shown in Fig. 2 with the controller given in Section 3 and assuming the parameters as shown in Table 2. The dc side of the proposed architecture is connected to a receiving end of 4 kV dc voltage through a transmission impedance.

First, the effect of capacitance value on the output voltage and the capacitor ripple voltage magnitudes is investigated in the presented simulation study. Then, a simulation case study of the overall system under variable wind speed is introduced.

4.1 Effect of dc-link capacitances on system performance

To investigate the effect of capacitor design on the system performance, the system performance is compared under two different values of the module capacitors: namely, 200 and 50 mF. The capacitance is relatively high because the generator phase voltage is low (200 V peak) while the phase current is relatively high (3 kA peak). The corresponding simulation results for these two values are shown in Figs. 5 and 6, respectively, assuming a fundamental output frequency of 50 Hz and the induced electromotive force (EMF) of phase 'A' is taken as a reference (i.e. zero-phase angle).

The modulating signals for both cases are shown in Figs. 5*a* and 6*a*. Figs. 5*b* and 6*b* show that the capacitor voltages are balanced in both cases, and the per-phase dc voltages are balanced as well, and their summation equals to the total dc-link voltage of the proposed converter. The capacitor ripple voltage magnitudes mainly depend on the magnitude of phase currents and the selected capacitances. As a result, the voltage fluctuations in the case of low dc-link capacitances are higher, which results in a higher possible fundamental output voltage. To have the same output voltage in both cases, the peak value of the modulating signals in case of low dc-link capacitances will be lower, as depicted by Figs. 5*a* and 6*a*.

The phase currents in both cases are shown in Figs. 5*c* and 6*c*. It is clear that the currents are identical and their peak magnitude equals the absolute of quadrature current reference $|i_q^*|$ (i.e. 3000 A), which confirms successful current tracking of the proposed controller.

The output phase voltage and the emf induced voltage of phase 'A' for both cases are shown in Figs. 5*d* and 6*d* as well. It is clear that the fundamental component of the phase voltage (v_a) is identical in both cases, which is expected for the same current reference and per-phase machine impedance.

Finally, Figs. 5*f* and 6*f* show the generator ac-side power and the dc-side power in both cases. It is clear that the ac-side power is higher than the dc-side power as the power flow is from the ac side to the dc side (i.e. rectification mode). The power difference represents the system losses (2.5% losses in the presented case).

The dc-side power in case of low capacitance has an oscillatory component as a reflection to the dc current ripple as shown in Fig. 6*e*.

Figs. 5*e* and 6*e* show the dc-link voltage and current in both cases. It has to be noted that the converter dc voltage is constant in both cases apart from the capacitance value is low or high. On the other hand, the dc-link current ripple magnitude in case of low capacitance value is higher as expected. Smoother current can be obtained by employing a smoothing reactor at the dc side.

It is worth mentioning that the total capacitor stored energy is likely more important than the absolute capacitance value in order to quantify the capacitor volume from a practical perspective. Practical experience advises that a total capacitor sorted energy of 30–40 kJ/MVA is acceptable in designing practical modular MMCs [32, 33]. This energy can be simply calculated from

$$E = \frac{1}{2} N_c C V_c^2 \tag{3}$$

where C is the capacitance, V_c is the average capacitor voltage, and N_c is the total number of capacitors.

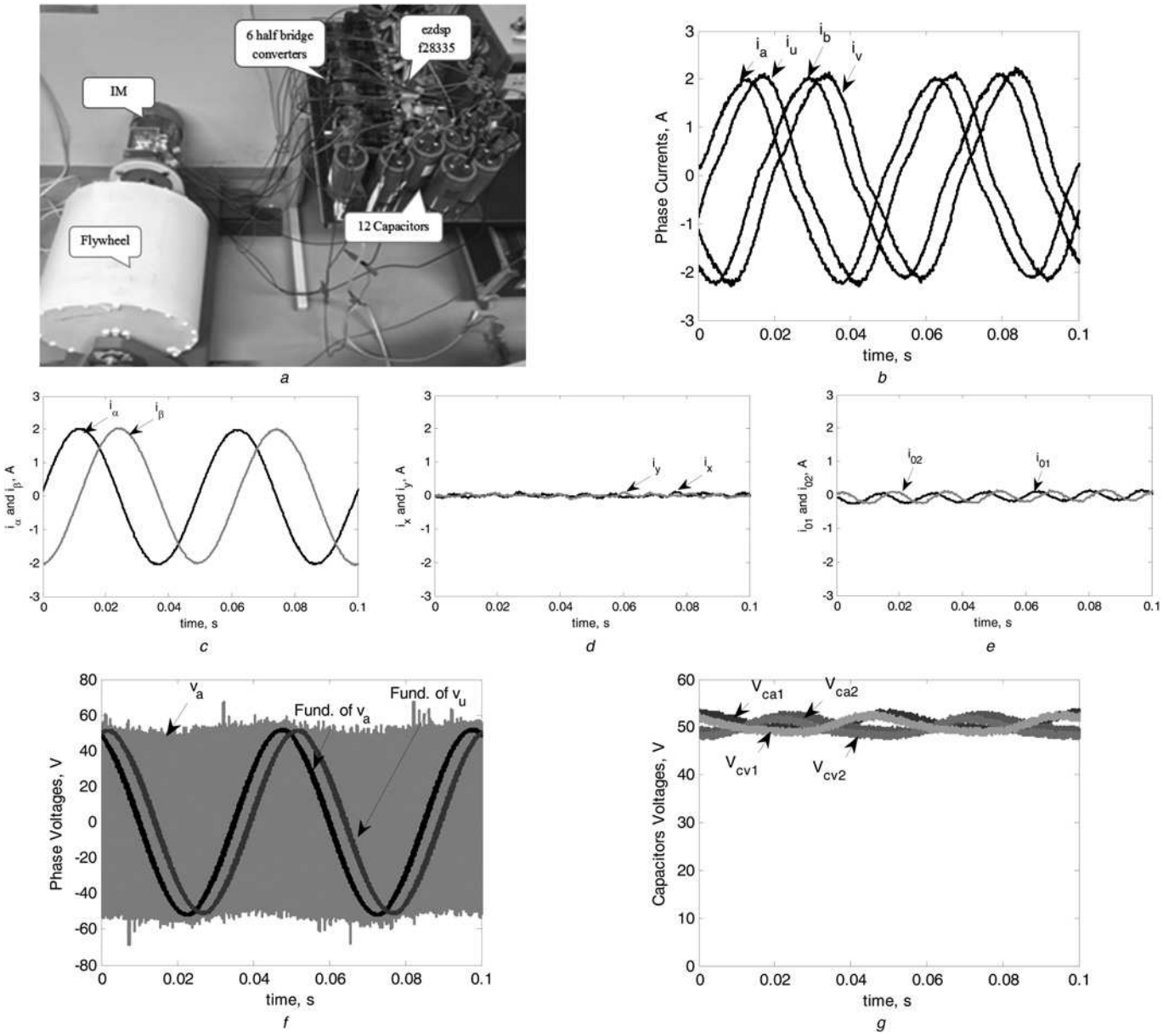

Fig. 8 *Experimental validation*

a Experimental rig
b Phase currents for phases (*a*, *u*, *b*, and *v*)
c $\alpha\beta$ Components of the stator currents
d *xy* Components of the stator currents
e Zero sequence components of stator currents
f Filtered phase voltages v_a and v_u
g Capacitors' voltages of phases (*a* and *v*)

For the presented simulation case study, the corresponding energy stored equals ~80 and 20 kJ/MVA for the 200 and 50 mF capacitors, respectively. Hence, the total energy stored in the 50 mF case is within the acceptable practical range, while providing an acceptable system performance.

4.2 System dynamic performance

In this section, the system performance is presented assuming a variable wind speed profile. Generally, as the wind speed changes, the optimum MPP point changes, which yields a variable quadrature reference current component (i_q^*). The effect of speed change on the dynamic performance is investigated by simulating the system, assuming that the generator speed linearly varies from 1 pu at $t = 1$ s to 0.8 pu at $t = 1.1$ s. The simulation results are shown in Fig. 7, assuming a value of 200 mF for all capacitors. Fig. 7*a* shows that the magnitude of the modulating signals decreases with the speed reduction. Fig. 7*b* shows the effect of the speed reduction on the capacitor voltages. It is clear that the capacitors' voltage ripple magnitude decreases with the reduction

Table 3 IM ratings and parameters

rated phase voltage, V	100
rated power, kW	1
rated frequency, Hz	50
full-load current, A	2.5
rated speed, rpm	960
stator resistance, Ω	6.1
stator leakage reactance, Ω	7.75
rotor referred resistance, Ω	5.155
rotor referred reactance, Ω	7.75
magnetising reactance, Ω	75
number of pole pairs	6

IET Electr. Power Appl., 2017, Vol. 11, Iss. 6, pp. 981–990

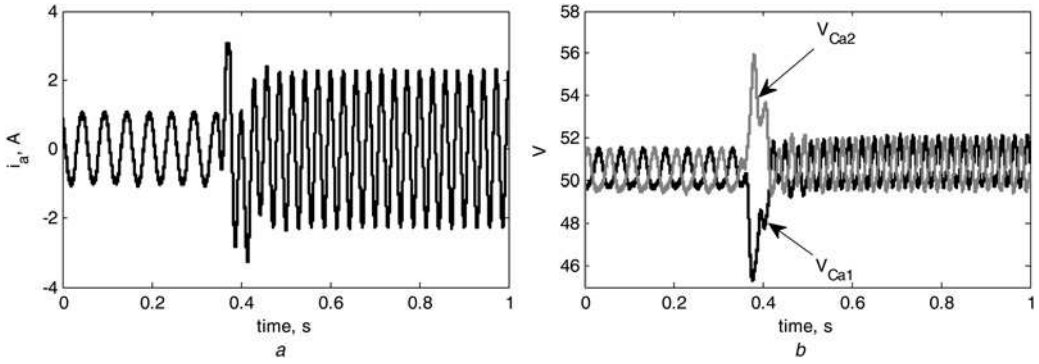

Fig. 9 *Experimental validation (Cont.). Effect of the current and frequency variation on the capacitors' voltages*

a Current of phase 'A'
b Voltages of phase 'A' capacitors

in the phase current (i_q^*) to $(0.8)^2$ pu, as shown in Fig. 7*c*. Finally, the variations of the ac-side and dc-side powers are shown in Fig. 7*d*. The input ac power drops to $(0.8)^3$ pu when speed decreases to 0.8 pu, which is expected as the mechanical power of the PMSG (P_m) is proportional to ω_m^3.

5 Experimental validation

In this section, since the generator type is not critical to properly assess the proposed converter, an existing 1 kW asymmetrical six-phase IM-based flywheel energy storage system is used for experimental validation as shown in Fig. 8*a*. Besides, though the proposed winding topology is proposed for wind generator, it can be also used in motoring mode of operation. The six-phase IM drives a flywheel system, which allows for a bidirectional power flow. The IM ratings and parameters are given in Table 3. A 600 V programmable dc supply is used as a dc link for the proposed converter. About 12 4700 μF/450 V capacitors are used with the six half-bridge converters.

The control is carried out using a digital signal processor board ezdsp F28335. The involved half-bridge converters are controlled using sinusoidal PWM with a switching frequency of 5 kH. Since the available dc supply is limited to 600 V, the maximum machine root mean square phase voltage will be limited to 35 V. Therefore, the machine will be tested at a lower stator frequency of 25 Hz.

To investigate the system performance under generation mode, the flywheel system was first operated under the motoring mode to accelerate it until the no load speed corresponding to a stator frequency of 25 Hz at a unity modulating signal peak. To reverse the power flow, the machine frequency is suddenly reduced with a step change to 20 Hz, and a suitable resistor is connected across the dc supply to provide a path for the pumped current from the machine into the dc bus. This sudden change in the stator frequency, with the high rotor inertia that emulates the effect of the wind turbine, forces the IM to operate in the generation mode until speed ceases down to a lower speed.

Fig. 8 shows the experimental results for this case during the discharging period directly after the frequency step change. Fig. 8*b* shows four out of the six phase currents, while the corresponding $\alpha\beta$ and xy current components are shown in Figs. 8*c* and *d*, respectively. It is clear that the phase currents experience harmonic distortion. Fig. 8*e* shows the bidirectional zero sequence component, which causes a notable phase current distortion due to an induced third harmonic zero sequence component, as clear from Fig. 8*b*. This notable harmonic component is mainly due to inverter asymmetries, as simple PWM technique is employed, and the relatively low machine zero sequence impedance. Since an open-loop control is adopted for experimental investigation, the zero sequence component was relatively high. This current component can be highly suppressed with closed-loop current control [19].

The filtered phase voltage of the first phase of each three-phase set is shown in Fig. 8*f*, whereas the capacitors' voltages are shown in Fig. 8*g*, which are clearly balanced and have equal average values of 600/12 = 50 V.

After the flywheel system reaches its steady-state condition, the frequency of the applied voltage has a step change from 20 to 40 Hz to show the effect of current and frequency variations on the capacitors' voltages. The corresponding experimental results for this case are shown in Fig. 9. The frequency of the capacitor voltage ripple depends on the stator current frequency, whereas its magnitude depends on both current magnitude and frequency. Interestingly enough, the average capacitor voltage level is independent of both frequency and current magnitude, while voltage balancing is also maintained.

On the basis of the obtained results, though simple *V/f* open-loop control is employed, the system performance was accepted. That was clear from voltage balancing under different loading conditions and balanced machine phase currents. Closed-loop control proposed in Section 3 would, therefore, enhance the system dynamics.

6 Conclusion

In this paper, a new WECS for integrating multi-MW multi-phase PMSGs with dc grid has been proposed. The proposed architecture consists of series-connected multi-half-bridge modules with a boosting gain from ac to dc sides equals $2m$, where m is the number of generator phases. Besides, the proposed approach can effectively provide a transformerless operation while employing relatively low-voltage semiconductor switches, which enhances the system efficiency, simplicity, and cost. Although the required capacitance value for different converter modules seems relatively high for high-power ratings, the voltage rating of such capacitors will be low, yielding an acceptable value of the total capacitor stored energy when compared with design values for practical modular MMCs. The effect of the dc-link capacitance on the performance has been also investigated through a detailed simulation study. It has been shown that a lower capacitance can be used with an enhanced fundamental output voltage at the cost of a higher dc-link ripple current. Hence, a compromise between the minimum selected capacitance and the acceptable performance indices should be made in the design phase based on the voltage and power levels. To improve the fault tolerant capability of the proposed architecture, additional redundant modules maybe employed to replace fault modules. Generally, these redundant modules will be bypassed during normal operating condition. Finally, simulation and experimental results validated the presented claims.

7 Acknowledgments

This publication was made possible by GSRA grant 2-1-0609-14027 from the Qatar National Research Fund (QNRF, a member of Qatar Foundation). The statements made herein are solely the responsibility of the authors.

8 References

1 Yaramasu, V., Wu, B., Sen, P.C., *et al.*: 'High-power wind energy conversion systems: state-of-the-art and emerging technologies', *Proc. IEEE*, 2015, **103**, (5), pp. 740–788

2 Gjerde, S.S., Olsen, P.K., Ljøkelsøy, K., *et al.*: 'Control and fault handling in a modular series-connected converter for a transformerless 100 kV low-weight offshore wind turbine', *IEEE Trans. Ind. Appl.*, 2014, **50**, (2), pp. 1094–1105

3 Chunkag, V., Kanthaphayao, Y., Kamnarn, U.: 'Distributed control system for a parallel-connected AC/DC converters', *IET Power Electron.*, 2013, **6**, (3), pp. 446–456

4 Zhang, X., Chen, J., Ma, Y., *et al.*: 'Bandwidth expansion method for circulating current control in parallel three phase PWM converter connection system', *IEEE Trans. Power Electron.*, 2014, **29**, (12), pp. 6847–6856

5 Ge, B., Lu, X., Yu, X., *et al.*: 'Multiphase-leg coupling current balancer for parallel operation of multiple MW power modules', *IEEE Trans. Ind. Electron.*, 2014, **61**, (3), pp. 1147–1157

6 Ge, B., Peng, F.Z.: 'Current balancer-based grid-connected parallel inverters for high power wind-power system', *Int. Trans. Electr. Energy Syst.*, 2014, **24**, pp. 108–124

7 Liao, Y.H., Chen, H.C., Cheng, H.C., *et al.*: 'A novel control strategy of circulating currents in paralleled single phase boost converters with different power sharing for microgrid applications', *IEEE Trans. Ind. Appl.*, 2014, **50**, (2), pp. 1304–1312

8 Gohil, G., Maheshwari, R., Bede, L., *et al.*: 'Modified discontinuous PWM for size reduction of the circulating current filter in parallel interleaved converters', *IEEE Trans. Power Electron.*, 2015, **30**, (7), pp. 3457–3470

9 Li, R., Xu, D.: 'Parallel operation of full power converters in permanent-magnet direct-drive wind power generation system', *IEEE Trans. Ind. Electron.*, 2013, **60**, (4), pp. 1619–1629

10 Ko, Y.J., Lee, K.B., Lee, D.C., *et al.*: 'Fault diagnosis of three-parallel voltage-source converter for a high-power wind turbine', *IET Power Electron.*, 2012, **5**, (7), pp. 1058–1067

11 Lyu, J., Zhang, J., Cai, X., *et al.*: 'Circulating current control strategy for parallel full-scale wind power converters', *IET Power Electron.*, 2016, **9**, (4), pp. 639–647

12 Hu, Y., Zeng, R., Cao, W., *et al.*: 'Design of a modular, high step-up ratio DC–DC converter for HVDC applications integrating offshore wind power', *IEEE Trans. Ind. Electron.*, 2016, **63**, (4), pp. 2190–2202

13 Gandomkar, A., Parastar, A., Seok, J.K.: 'High-power multilevel step-up DC/DC converter for offshore wind energy systems', *IEEE Trans. Ind. Electron.*, 2016, **63**, (12), pp. 7574–7585

14 Ng, C., Parker, M., Ran, L., *et al.*: 'A multi- level modular converter for a large, light weight wind turbine generator', *IEEE Trans. Power Electron.*, 2008, **23**, (3), pp. 1062–1074

15 Parker, M., Ng, C., Ran, L., *et al.*: 'Power control of direct drive wind turbine with simplified conversion stage transformerless grid interface'. Proc. 41st Int. UPEC, Newcastle upon Tyne, UK, September 2006, vol. 1, pp. 65–68

16 Carmeli, M.S., Castelli-Dezza, F., Marchegiani, G., *et al.*: 'Design and analysis of a medium voltage DC wind farm with a transformer-less wind turbine generator'. 2010 XIX Int. Conf. on Electrical Machines (ICEM), Rome, 2010, pp. 1–6

17 Wang, M., Hu, Y., Zhao, W., *et al.*: 'Application of modular multilevel converter in medium voltage high power permanent magnet synchronous generator wind energy conversion systems', *IET Renew. Power Gener.*, 2016, **10**, (6), pp. 824–833

18 Yaramasu, V., Wu, B.: 'Predictive control of a three-level boost converter and an NPC inverter for high-power PMSG-based medium voltage wind energy conversion systems', *IEEE Trans. Power Electron.*, 2014, **29**, (10), pp. 5308–5322

19 Gonzalez, I., Dura, J., Che, H.S., *et al.*: 'Fault-tolerant efficient control of six-phase induction generators in wind energy conversion systems with series–parallel machine-side converters'. Seventh IET Int. Conf. on Power Electronics, Machines and Drives (PEMD 2014), Manchester, 2014, pp. 1–6

20 Yuan, X., Li, Y., Chai, J.: 'A transformerless modular permanent magnet wind generator system with minimum generator coils'. 2010 25th Annual IEEE Applied Power Electronics Conf. and Exposition (APEC), Palm Springs, CA, 2010, pp. 2104–2110

21 Gonzalez-Prieto, I., Duran, M.J., Barrero, F., *et al.*: 'Impact of post-fault flux adaptation on six-phase induction motor drives with parallel converters', *IEEE Trans. Power Electron.*, 2017, **32**, (1), pp. 515–528

22 Gonzalez-Prieto, I., Duran, M.J., Che, H.S., *et al.*: 'Fault-tolerant operation of six-phase energy conversion systems with parallel machine-side converters', *IEEE Trans. Power Electron.*, 2016, **31**, (4), pp. 3068–3079

23 Duran, M.J., Prieto, I.G., Bermudez, M., *et al.*: 'Optimal fault-tolerant control of six-phase induction motor drives with parallel converters', *IEEE Trans. Ind. Electron.*, 2016, **63**, (1), pp. 629–640

24 Asplund, G.: 'Tapping power from a HVDC transmission system'. US Patent US2010/0091527A1, April 2010

25 EL-Refaie, A.: 'Fractional-slot concentrated-windings synchronous permanent magnet machines: opportunities and challenges', *IEEE Trans. Ind. Electron.*, 2010, **57**, (1), pp. 107–121

26 Potgieter, J., Kamper, M.: 'Torque and voltage quality in design optimization of low-cost non-overlap single layer winding permanent magnet wind generator', *IEEE Trans. Ind. Electron.*, 2012, **59**, (5), pp. 2147–2156

27 Williamson, A.C., Spooner, E., Thompson, L.: 'Large modular PM generators'. *IEE Colloq. New Topologies Permanent Magnet Mach. (Digest No: 1997/090)*, 1997, pp. 1–6

28 Jia, S., Qu, R., Li, J., *et al.*: 'Study of direct-drive permanent-magnet synchronous generators with solid rotor back iron and different windings', *IEEE Trans. Ind. Appl.*, 2016, **52**, (2), pp. 1369–1379

29 Wu, B., Yongqiang, L., Zargari, N., *et al.*: 'Power conversion and control of wind energy systems' (IEEE Press, John Wiley, 2011)

30 Ebrahimi, M., Ali Khajehoddin, S.: 'A simple DQ current controller for single-phase grid-connected inverters'. 2015 IEEE Applied Power Electronics Conf. and Exposition (APEC), 2015, pp. 2840–2845

31 Elserougi, A., Massoud, A.M., Abdel-Khalik, A.S., *et al.*: 'A grid-connected HVDC shunt tap based on series-input parallel-output DC–AC multi-module 2-level voltage source converters'. 2015 IEEE Eighth GCC Conf. and Exhibition (GCCCE), 2015, pp. 1–5

32 Jovcic, D., Ahmed, K.: 'High voltage direct current transmission: converters, systems and DC grids' (John Wiley, 2015), p. 193

33 Jacobson, B., Karlsson, P., Asplund, G., *et al.*: 'VSC-HVDC transmission with cascaded two-level converters'. Presented at the CIGRE Session, Paris, France, 2010